Article

PLLA Nanosheets for Wound Healing: Embedding with Iron-Ion-Containing Nanoparticles

Aslan Mussin , Ali Al-Julaih , Neli Mintcheva , Delvin Aman , Satoru Iwamori , Stanislav O. Gurbatov , Abhishek Bhardwaj , Sergei A. Kulinich *

Posted Date: 7 August 2023

doi: 10.20944/preprints202308.0512.v1

Keywords: PLLA nanosheets; laser ablation in liquid; Fe-containing nanoparticles; metal-ion release; burn wound healing

Article

PLLA Nanosheets for Wound Healing: Embedding with Iron-Ion-Containing Nanoparticles

Aslan Mussin [1], Ali A. AlJulaih [1], Neli Mintcheva [1,2], Delvin Aman [3], Satoru Iwamori [1,4], Stanislav O. Gurbatov [5], Abhishek Bhardwaj [6] and Sergei A. Kulinich [1,4,*]

[1] Department of Mechanical Engineering, Tokai University, Hiratsuka, Kanagawa 259-1292, Japan

[2] Department of Chemistry, University of Mining and Geology, Sofia 1700, Bulgaria

[3] Catalysis Division, Petroleum Refining Department, Egyptian Petroleum Research Institute, Cairo 11727, Egypt

[4] Research Institute of Science and Technology, Tokai University, Hiratsuka, Kanagawa 259-1292, Japan

[5] Institute of Automation and Control Processes, Far Eastern Branch, Russian Academy of Science, Vladivostok 690041, Russia

[6] Department of Environmental Science, Amity University, Gwalior, Madhya Pradesh 474005, India

* Correspondence: skulinich@tokai-u.jp (S.A.K.)

Abstract: This article reports on polymer (PLLA, poly(L-lactic acid)) nanosheets incorporated with Fe-ion nanoparticles, aiming at using the latter nanoparticles as a source to release Fe ions. Such Fe ions should facilitate burn wound healing when such nanosheets are applied as a biomedical tissue on skin. Laser ablation in liquid phase was used to produce Fe-containing nanoparticles that after incorporation into PLLA nanosheets would release Fe ions upon immersion in water. Unlike most of iron-oxide nanostructures that are poorly soluble, such nanoparticles prepared in chloroform were found to have water solubility, as they were shown by XPS to be based on iron chloride and oxide phases. After incorporation into PLLA nanosheets, the ion –release test demonstrated that Fe ions could be released successfully into water at pH 7.4. Incorporation with two different metal ions (Fe and Zn) was also found to be efficient as both types of ions were demonstrated to be released simultaneously and with comparable release rates. The results imply that such polymer nanosheets show promise for biomedical applications as potential patches for healing of burn wounds.

Keywords: PLLA nanosheets; laser ablation in liquid; Fe-containing nanoparticles; metal-ion release; burn wound healing

1. Introduction

Wounds are defined as damage or disturbance of normal anatomical structure and function of skin resulted from pathological processes that begin internally or externally to the involved organs [1,2]. Among different types of wounds, burn ones are known typically to need long-lasting and complex treatment to provide, support and accelerate their healing [3–13]. An ideal wound dressing used for their treatment should accelerate one or several stages of the healing processes including the inflammatory phase, the migratory phase, the proliferative phase, and the remodeling phase. Nowadays, a variety of wound dressings are available and still widely used to treat such wounds [3–10,12,13]. And even though the characteristics of "ideal" dressings for wound treatment are well known, such ultimate dressings are still difficult to be realized within the same material [4–13]. It is still challenging, if ever possible, to realize an optimal combination of desired properties in one wrapping material, implying that new materials with improved characteristics are still highly anticipated. In parallel, incorporation of metal ions such as Mg, Zn, Fe and Cu is believed to be beneficial for efficient wound healing [2,4,5,11,14–16], however, very little progress was achieved in this direction thus far.

Preprints (www.preprints.org) | NOT PEER-REVIEWED | Posted: 7 August 2023 doi:10.20944/preprints202308.0512.v1

Free-standing ultra-thin films (also known as nanosheets, NSs) of several biodegradable polymers (e.g., poly(L-lactic acid), PLLA) have been recently reported as efficient materials to cover burn wounds, with the ability to adhere to any shape and protect wounds for days without the need for daily replacement [11,17–20]. As wound wrapping materials, such NSs are: (1) inexpensive and relatively easy to prepare; (2) highly adhesive to virtually any surface with any shape; (3) permeable for water and air and biodegradable; (4) good as barriers for infection and dirt, and so on [11,17–20]. Embedding such inexpensive and biodegradable polymer NSs with ions of crucial metals that can be released upon contacting the wound surface is therefore believed to enhance their performance as burn-wound dressings further [11,17–20].

Embedding PLLA nanosheets with sources of metal ions, such as Mg, Zn, Fe and Cu, is believed to provide additional merits to such biomedical materials as these ions were reported to be essential for improved wound healing [2,11,14–16]. In our previous work, we prepared PLLA NSs incorporated with Zn-containing NPs and demonstrated that NPs based on both $ZnCl_2$ and ZnO can be efficient source of Zn ions that can be released from PLLA NSs in contact with water medium [11]. Since embedded NPs should be sufficiently soluble in water, we used ZnO and $ZnCl_2$ based NPs which were then incorporated into PLLA NSs by means of spin-coating. The produced NSs were characterized and their ability to release Zn ions was tested after immersion in water at pH of 7.4 and 37 °C [11]. To prepare such Zn-containing NPs, we applied the laser ablation in liquid (LAL) phase, which is a convenient laboratory technique permitting to prepare diverse nanomaterials (including metallic and metal oxide NPs, among others) with easy parameter control and at laboratory scale [21–35] (see Figure 1).

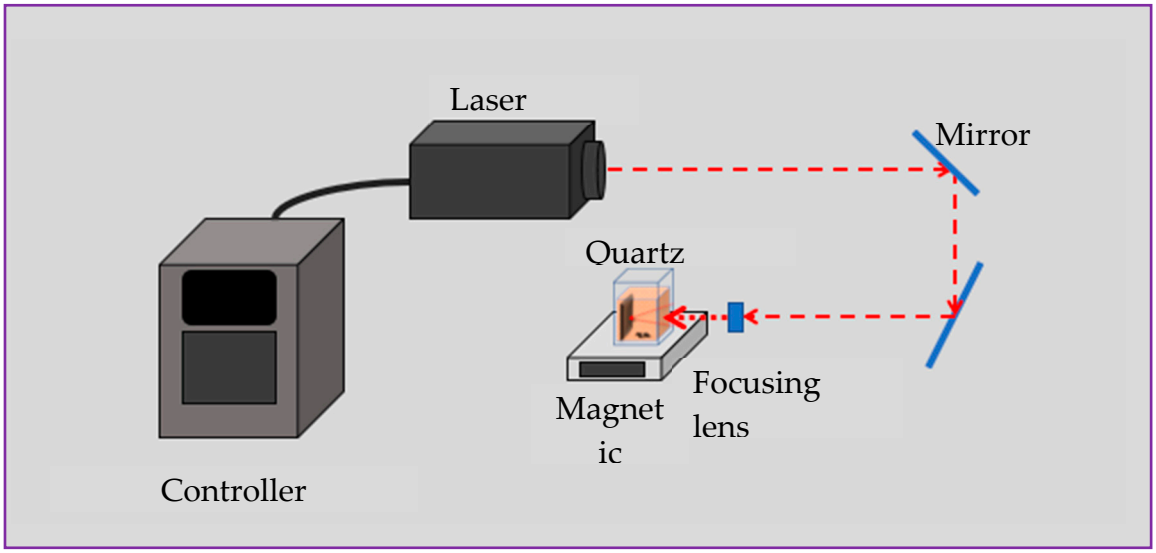

Figure 1. Setup with ns-pulsed laser used to produce nanoparticles via ablating iron plate in chloroform.

Encouraged by the previous results, herein we apply the same method to produce Fe-containing NPs as nano-reservoirs for Fe ions that can be released from their PLLA matrix (NSs) upon embedment. We also employed LAL in chloroform to produce Fe-containing NPs, expecting such NPs to be based on chloride phases, similar to our previous work on Zn ablation in chloroform [11]. When LAL is applied to Fe targets in water or air, the product is known to be based on various iron oxides/hydroxides [22,33,34,36–40]. Based on the literature, all major Fe oxides are known to be insoluble in water, which is why we decided to rely on Fe chloride based nanomaterials, whose formation was expected as a result of Fe ablation in chloroform.

Thus, this work took advantage of the LAL as a method to prepare Fe-containing NPs which would be soluble in water. Two types of Fe-Cl NPs were prepared at different laser parameters and then characterized, after which they were incorporated into PLLA NSs. For comparison, we also used

 doi:10.20944/preprints202308.0512.v1

commercially available iron oxide NPs (Fe_2O_3), which were also embedded into PLLA nanosheets. As a next stage, we studied how the prepared NSs released Fe ions, the dynamics that should be of high importance when such biomedical materials are applied for wound healing. Finally, we demonstrate NSs incorporated with two types of NPs that contain two metal ions (Fe and Zn), as well as their ion release.

Hence, the work paves an avenue for easy-to prepare and low-cost new-generation biomedical materials, i.e., bio-friendly polymer nanosheets incorporated with nano-containers that can release metal ions aiming at accelerating wound healing. Such materials are highly anticipated for multiple biomedical applications, especially as inexpensive wound-dressing in surgery and regenerative medicine.

2. Experimental Part

2.1. Chemicals and Materials

Iron plates (99.8% pure) were supplied by Nilaco Corp. Deionized water, chloroform (99.0% pure) and ethanol (99.5%) were all purchased from Wako Pure Chemical Industries (Japan). Phosphate-buffered saline solution (PBS) was purchased from Merk, polyvinyl alcohol (PVA) was acquired from Kanto Chemical Co. (Japan), while Fe_2O_3 and ZnO NPs (with sizes below 50 nm and 20-25 nm, respectively) were supplied by Sigma-Aldrich and Wako Pure Chemical Industries, respectively. Finally, PLLA (Mw: 80–100 kDa) was supplied by Polysciences, Warrington, PA (USA).

2.2. Preparation of Fe-Containing NPs

Laser ablation in liquid (LAL) is a convenient laboratory technique to generate NPs with different morphology, sizes and chemistry [21–29,33,34,41–44]. In this method, laser beam is typically focused on a solid target (or powder dispersed in liquid), and its pulses ablate (or modify) the target to produce nanostructures with morphology, size and chemistry that depend on the used liquid and target, as well as on the properties of laser pulses applied [21,24–29,31–34,45]. This approach is attractive for research purposes since it is simple in use, inexpensive and consumes minimum chemicals, among other advantages. In this study, as we needed water-soluble NPs containing Fe ions, we applied LAL to ablate iron plate in chloroform, as this was expected to result in chloride-based NPs.

Unlike our previous work on $ZnCl_2$-based NPs generated via LAL [11], here we applied a nanosecond pulsed laser to ablate iron plates in chloroform. Samples A and B were prepared using a YAG laser operating at different pulse energy as described in Table 1.

Table 1. Description of Fe-containing colloids produced by ablating iron plat with ns-pulsed laser.

Sample	Ablation time (min)	Liquid medium	Pulse energy (mJ)
Sample A	20	Chloroform	30
Sample B	20	Chloroform	120

Iron metal plate with a thickness of 1.0 mm was cut into pieces 1.5 x 3.0 cm^2 in size which were then sonicated in ethanol for 5 min. After drying in air, the plates were placed in a quartz cuvette with 15 mL of chloroform. During ablation for 20 min, the produced colloids were magnetically stirred (Figure 1). A nanosecond pulsed Nd: YAG laser with the fundamental wavelength of 1064 nm was used for preparing iron-chloride based NPs, with the experimental setup being exhibited in Figure 1, while more details on both the setup and laser used can be found elsewhere [11,27,32,41,42].

2.3. Characterization of Prepared NPs

Preprints (www.preprints.org) | NOT PEER-REVIEWED | Posted: 7 August 2023 doi:10.20944/preprints202308.0512.v1

The prepared colloids of Fe-Cl containing NPs were first centrifuged at 16,000 rpm and then drop-cast on Si wafers for X-ray photoelectron spectroscopy (XPS) and X-ray diffraction (XRD) analyses or on C-coated Cu grids for transmission electron microscopy (TEM).

Morphology of obtained NPs and NSs were taken using scanning electron microscopy (SEM, S4800 from Hitachi, Japan), while XPS analysis was carried out on a PHI-1600 spectrometer (Physical Electronic Industries, USA). The recorded binding energy peaks were all corrected for charge shifting by referencing to the adventitious carbon C 1s line at 284.8 eV. In order to remove adventitious carbon from the sample surface, argon sputtering was applied, after which samples were analyzed. Quantification of the peaks was carried out by using the XPSPeak4.1 software, which permitted to curve-fit the peaks of elements comparing them with data already available in the literature.

TEM analysis was performed on a HF-2200 tool from Hitachi. The samples were prepared by pipetting as-prepared dispersions onto copper micro-grids and drying in air. The optical characteristics of NPs in colloids were studied using an UV-visible absorption spectroscope (UV-2450, Shimadzu). The NP size in the liquid state was measured using a nanoparticle analyzer by dynamic light scattering (DLS) technique.

2.4. Nanosheets Loaded with NPs and Their Analysis

Because chloroform is compatible as solvent for our spin-coating based approach to prepare PLLA NSs, NPs prepared in chloroform by ablation were ready for direct mixing with PLLA polymer followed by spin-coating [11,19,20]. Commercial Fe_2O_3 or ZnO NPs used for comparison, prior to further processing, were weighed and dispersed in chloroform, after which they were mixed with PLLA for further spin-coating as PLLA NSs.

Figure 2 shows schematically how NP-embedded PLLA NSs were prepared. NP dispersions in polymer solution of $CHCl_3$ were spin-coated onto a Si wafer coated with a water-soluble polymer, PV. After that, upon fast immersion in water, free-standing PLLA NSs were delaminated as PV dissolved in water. The amount of Fe-containing NPs in the PLLA-$CHCl_3$ solution was evaluated based on the weight loss of Fe plate evaluated after ablation. Because the produced NPs had a complex composition and had both Fe(II) and Fe(III) species, for simplicity, we used concentrations in moles per liter (of Fe atoms) to prepare PLLA NSs embedded with NPs from Samples A and B. If necessary, the as-prepared dispersions were diluted with chloroform to adjust their concentrations prior to mixing with PLLA and further spin-coating.

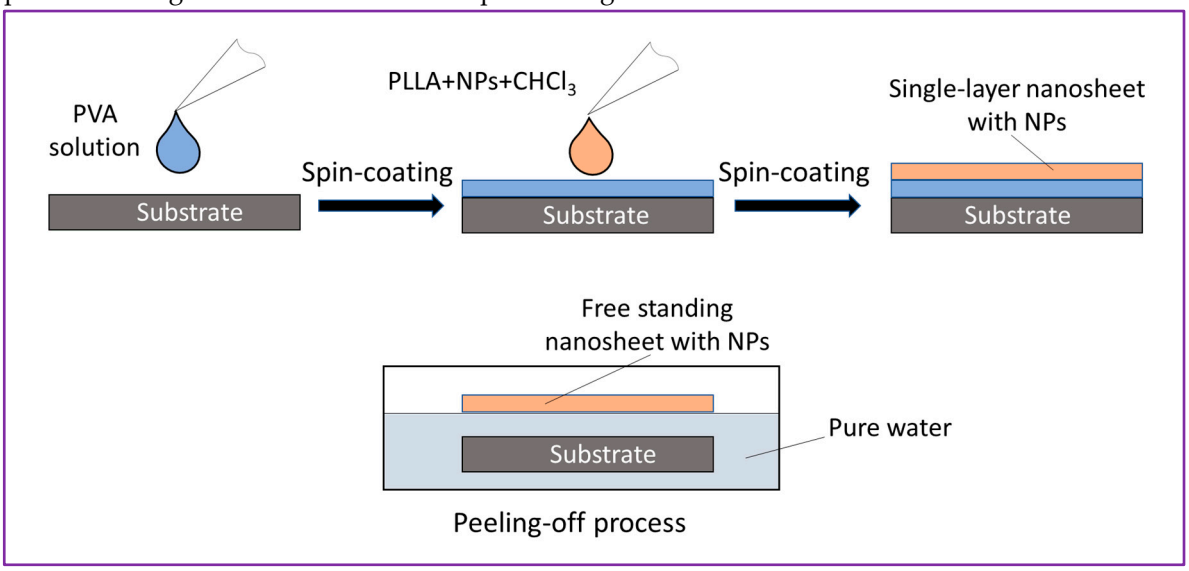

Figure 2. Fabrication of PLLA nanosheet incorporated with nanoparticles.

As seen in Figure 2, the PLLA NSs were prepared by spin-coating. For that, typically the concentration of the mixture was 10 mg of PLLA (as crystals) and 1 mL of LAL-generated colloid.

Preprints (www.preprints.org) | NOT PEER-REVIEWED | Posted: 7 August 2023 doi:10.20944/preprints202308.0512.v1

The substrate was spun for 20 s and dried on a hotplate at 70 °C for 90 s. By using a cutter, a light cut was then made on the substrate to form a sample of 3 x 3 cm^2, after which the substrate was immersed in water where it was moved from time to time with tweezers until the PLLA NS began to float (Figure 2). At this point, the pilled-off NP-incorporated NS was transferred onto a polyester mat (filter) to preserve its shape and for further storage (see Figure 3c).

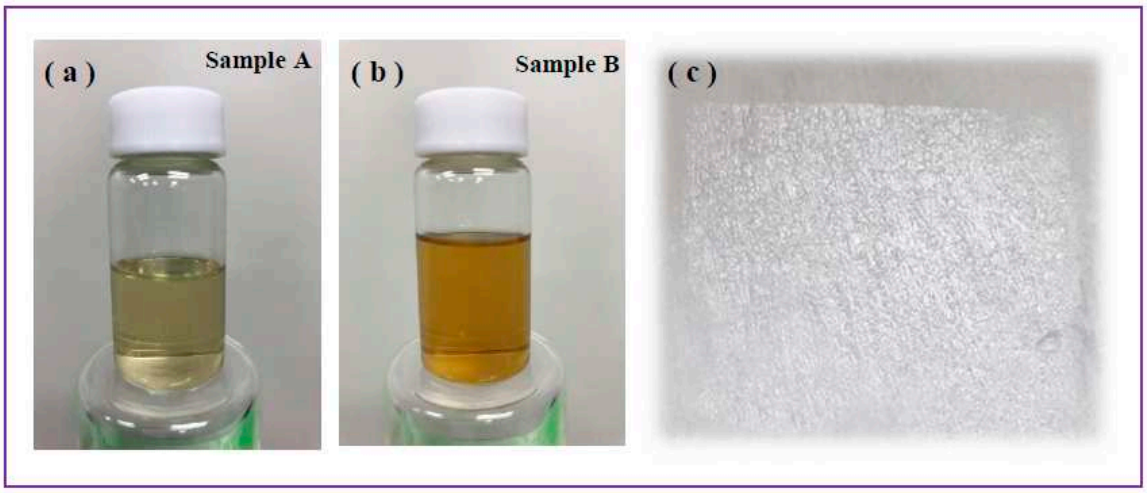

Figure 3. Colloids of Fe-containing NPs laser-generated in chloroform at 30 (a) and 120 mJ/pulse (b), and a PLLA nanosheet incorporated with such NPs (c) placed on polyester filter mat. The actual size of the NS in panel (c) is 3 cm x 3 cm.

2.5. Ion Release from NP-Embedded NSs

The release of metal ions from NS samples was studied by means of inductively coupled plasma mass spectroscopy (ICP-MS). The samples were immersed in flasks with 40 mL of PBS solution (pH 7.4) at 37 °C to simulate human's body conditions (see Figure 4). To analyze the concentration of Fe ions over time, aliquots of 1 mL were taken and analyzed after certain periods of time. To determine concentration of metal ion in analyzed solution, calibration curves were plotted for each analyzed element using standard solutions, as previously reported elsewhere [46–48]. After each sampling, a volume of 1 mL of PBS was added to the sample. For each sample, measurements were carried out in triplicate, after which the obtained results were averaged. Nanosheets incorporated with laser-ablated Fe-containing NPs, as well as their counterparts incorporated with commercially available ZnO and Fe_2O_3 NPs, were evaluated in terms of Fe or/and Zn ion release.

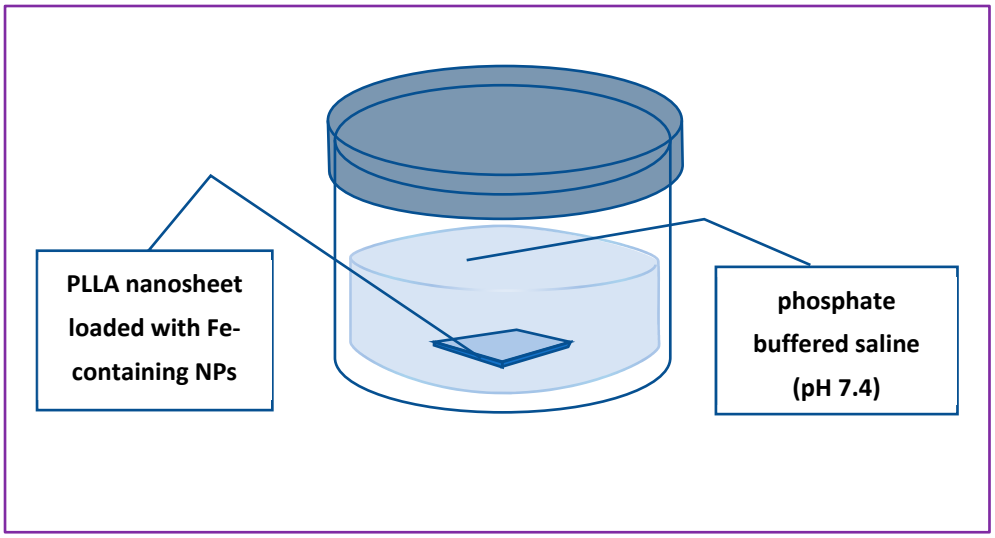

Preprints (www.preprints.org) | NOT PEER-REVIEWED | Posted: 7 August 2023 doi:10.20944/preprints202308.0512.v1

Figure 4. Experimental set-up used for ion-release test.

3. Results and Discussion

3.1. Fe-containing NPs prepared by LAL

Figure 3a,b shows the as-prepared colloids of Samples A (a) and B (b), while Figs.5,6 exhibit electron microscopy images of the same samples (Figures 5 and 6, respectively). As well seen in Figure 3a,b, yellow-brownish colloidal suspensions were obtained as a result of iron plate ablation in chloroform. The color of prepared colloids is predictably dependent on applied laser parameters, which is probably explained by the number, size and chemical composition of produced NPs. No significant temperature increase was detected during the whole ablation process, which agrees well with the literature (as ns-long pulses are known not to transfer much energy to the target and liquid medium [32,41,42]. Since Sample B was prepared using laser beam with higher pulse energy, it is reasonable that the concentration of produced NPs should be higher, in agreement with material loss observed by weighing iron plates after ablation in both cases.

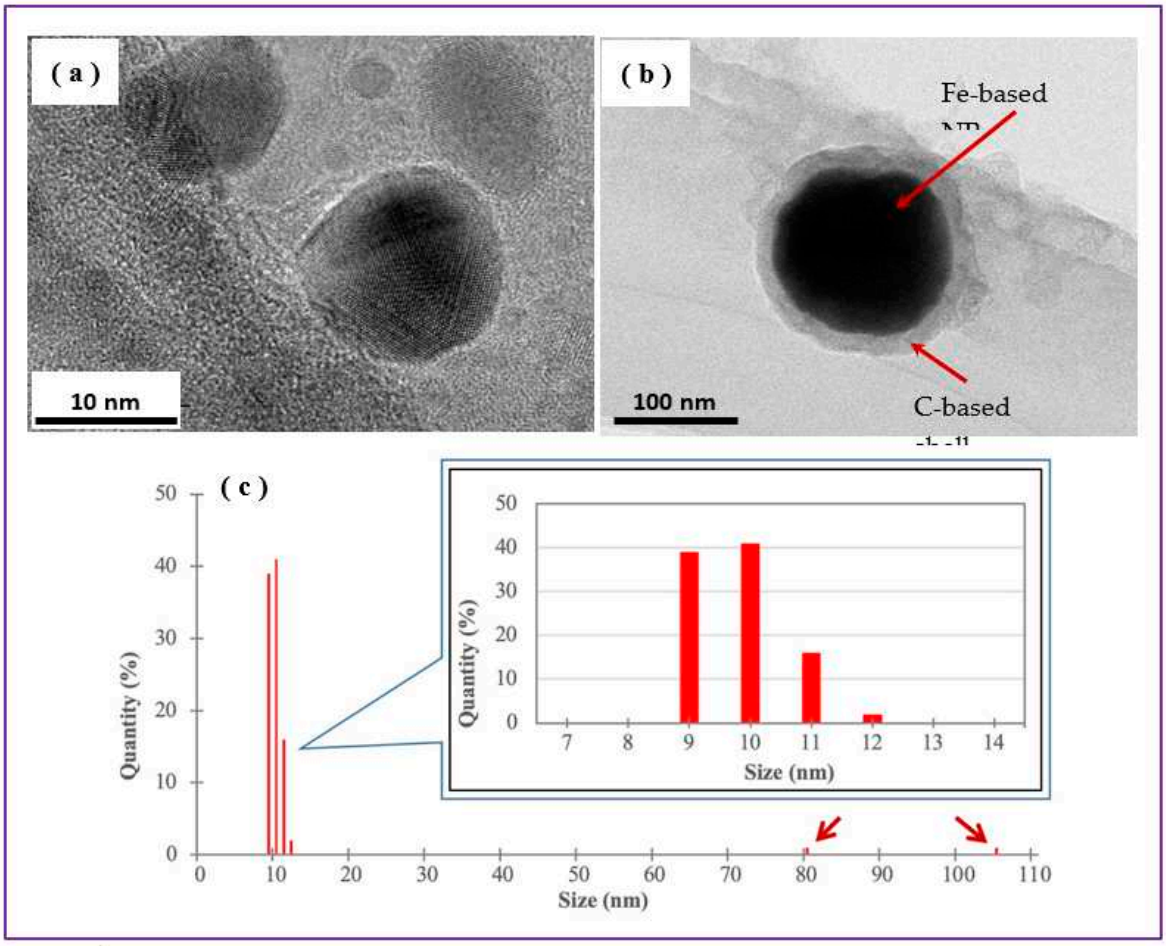

Figure 5. (a,b) TEM images of Fe-based NPs prepared at 30 mJ/pulse (Sample A): (a) small NPs and (b) bigger NP with C-based shell. (c) Histogram of size distribution of Fe-containing NPs as measured by DLS. Two red arrows in panel (c) indicate bars for NPs with sizes ~81 and ~106 nm.

Preprints (www.preprints.org) | NOT PEER-REVIEWED | Posted: 7 August 2023 doi:10.20944/preprints202308.0512.v1

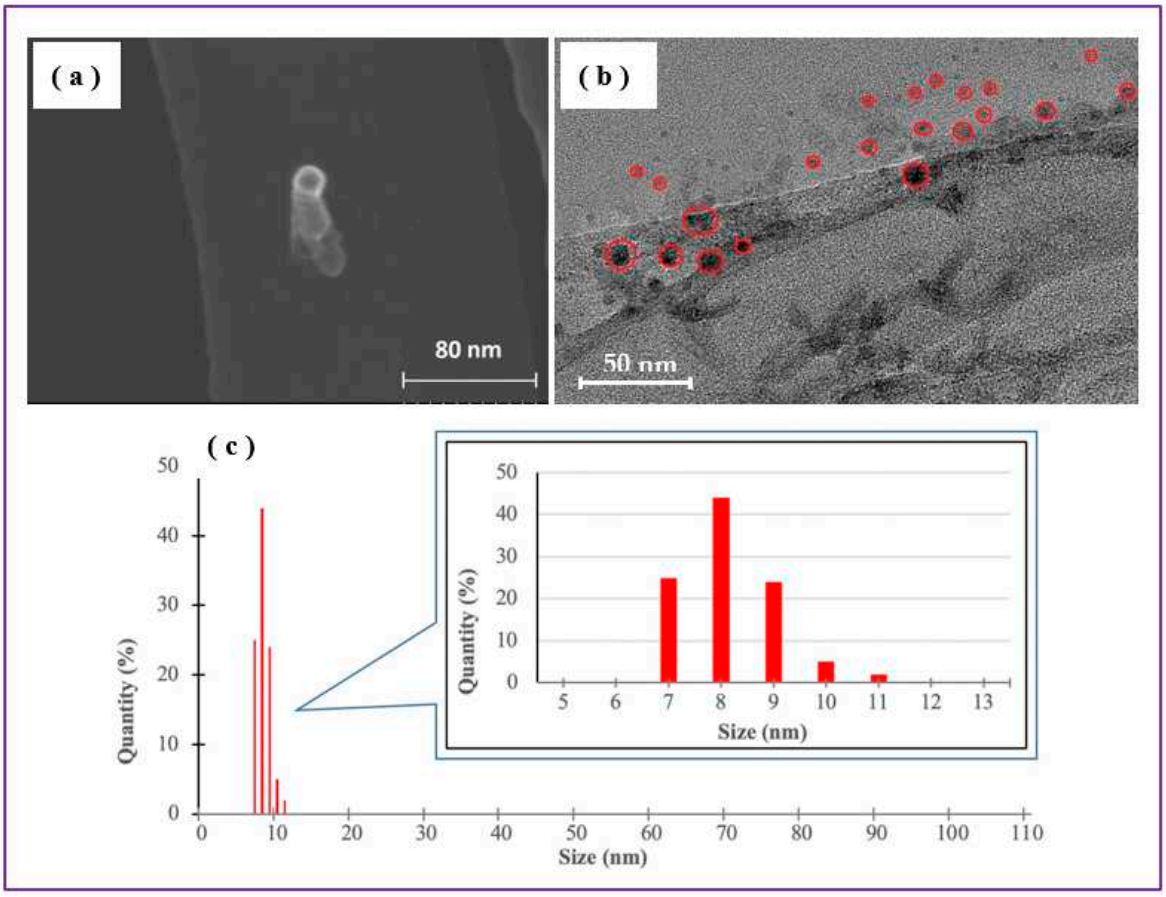

Figure 6. SEM (a) and TEM (b) images of Fe-based NPs prepared at 120 mJ/pulse (Sample B). (c) Histogram of size distribution of NPs in Sample B as measured by DLS.

Transmission electron microscopy was used to visualize the morphology and size distribution of generated NPs. It is seen that that Sample A prepared at 30 mJ/pulse had spherically-shaped NPs with sizes mainly between 7 and 12 nm with an average size around 10 nm (Figure 5c). At the same time, a small fraction of bigger NPs with sizes of 80-105 nm was also observed, as shown by arrows in Figure 5c. Graphite-like shell surrounding the core of some Fe-based NPs could be observed around bigger NPs (Figure 5b), which is believed to be explained by the pyrolysis of chloroform (as organic medium used) as high temperatures were reached locally in the ablation zone shortly after laser pulses hit the target.

Figure 6 shows that Fe-based NPs in Sample B (prepared at 120 mJ/pulse) had approximately same sizes as their counterparts produced at a lower pulse energy (30 mJ/pulse), being mainly within the range of 5-15 nm and with an average size of 10±2 nm (Figure 6c). The NPs are also spherically shaped, however, no bigger NPs of ~100 nm in size and with well-defined carbon-based shells were found in this sample. The absence of bigger NPs in the product produced at a higher pulse energy is not clear yet, as the entire mechanism of NP formation caused by ns-long laser pulses in chloroform medium is still to be studied. At this stage, we can postulate that probably bigger Fe-based NPs formed during ablation could be fragmented by secondary irradiation, especially because higher energy fluence was used to produce Sample B.

DLS is a technique that permits to evaluate the size distribution of NPs in dispersions. In Figures 5c and 6c, one can see the histograms of size distribution of NPs in Samples A and B, respectively. The sizes of most NPs in Figure 5c are seen to be within the range of 9-12 nm, while there is still a small number of NPs with sizes between 80 and 105 nm. This agrees well with TEM images presented in Figure 5a,b. For Sample B, its NPs are seen in Figure 6c to be somewhat smaller, within the range of 7 to 11 nm, which is also consistent with TEM and SEM images in Figure 6a,b. Importantly,

Preprints (www.preprints.org) | NOT PEER-REVIEWED | Posted: 7 August 2023 doi:10.20944/preprints202308.0512.v1

comparison of Figures 5 and 6 also permits to conclude that both samples consisted of NPs with sizes proper for embedment into PLLA NSs (which are typically thinner than 100 nm).

UV-visible absorption spectroscopic measurements were carried out on freshly prepared colloids. Typically, Fe-based NPs are known not to be easily identified by UV-visible spectroscopy because they lack sharp absorption bands in this spectral range [49], which makes accurate identification of NP forms by UV-visible spectra difficult. However, both samples are seen in Figure 7 to demonstrate absorption edge at wavelengths below 400 nm, which is consistent with the optical spectra of most oxidized iron phases (Figure 7) [50].

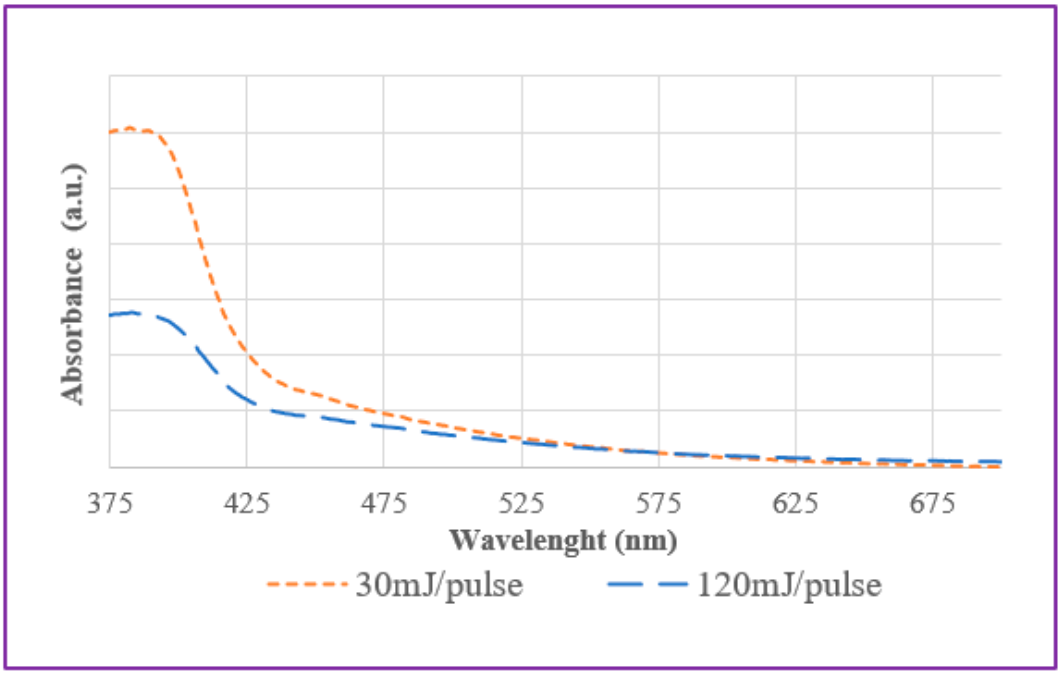

Figure 7. UV-visible spectra of Fe-based colloids prepared using ns-pulsed laser at 30 (orange) and 120 mJ/pulse (blue).

3.2. XPS analysis of prepared NPs

Figure 8 presents XPS Fe 2p spectra of Samples A (a) and B (b). Corresponding Cl 2p and O 1s spectra are shown in *Supplementary Materials* Figures S1 and S2, respectively. As iron is a transition metal, the Fe 2p spectra of both samples presented in Figure 8a,b demonstrate doublets, i.e., peaks Fe $2p_{3/2}$ (between ~705 and ~723 eV) and Fe $2p_{1/2}$ (between ~718 and ~735 eV). For brevity and convenience, below we only focus on the Fe $2p_{3/2}$ peaks which are easier to analyze and thus are more informative.

Preprints (www.preprints.org) | NOT PEER-REVIEWED | Posted: 7 August 2023 doi:10.20944/preprints202308.0512.v1

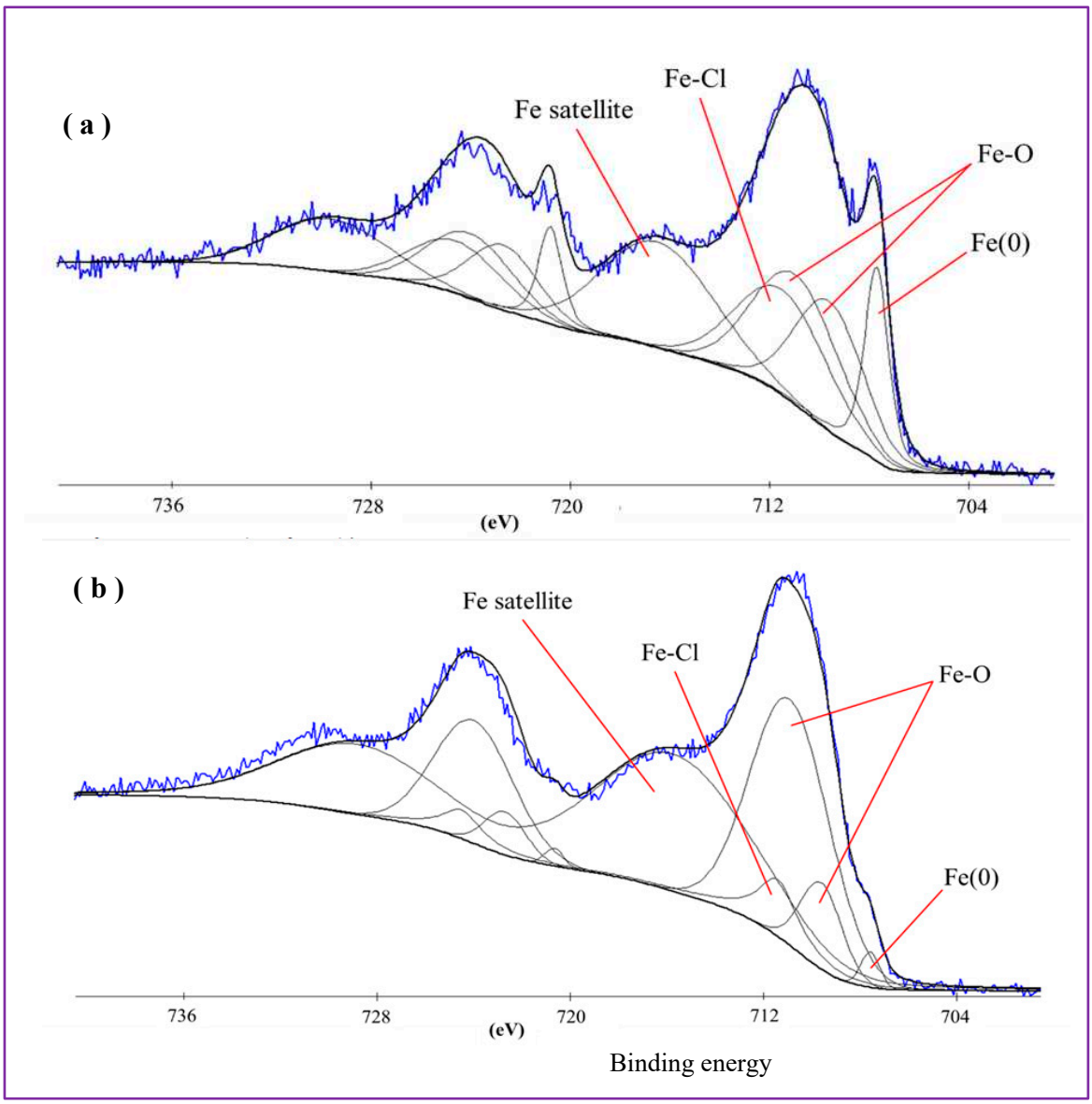

Figure 8. XPS Fe 2p spectra of Samples A (a) and B (b) prepared at 30 and 120 mJ/pulse, respectively.

Figure 8a presents the Fe 2p spectrum of Sample A, which was curve-fitted using several components. The peak at a lower binding energy (~708 eV) was assigned to metallic iron (Fe(0)), thus implying that the produced NPs were partially composed of non-oxidized metallic iron. It is reasonable to assume that: (i) the liquid medium we used (chloroform) is not a strong oxidizer; (ii) the graphitic shell found in TEM images to surround the core of some NPs could prevent their core from further oxidation; (iii) some metallic phase inclusions could also be embedded by NPs free of graphite shell too. This can explain the presence of Fe(0) species in the produced NPs. The wide peak observed between 709 and 715 eV was fitted with several components corresponding to Fe-Cl and Fe-O species. Note that because of close positions of Fe(II) and Fe(III) species (both oxides and chlorides), it was impossible to distinguish with certainty which of the two (or both) was present and dominated in the sample [22,33,34,37–40].

In Figure 8b, the XPS Fe2p spectrum of Sample B produced via ablation at 120 mJ/pulse is shown. In comparison with Figure 8a, the amount of metallic Fe in this sample is smaller than in its counterpart ablated at 30 mJ/pulse. This was expected as Fe(0) species are more likely to be oxidized when iron plate is ablated by pulses with higher energy, which should generate higher temperatures in the ablation zone. Moreover, the amount of oxidized forms of iron increases at increased laser

Preprints (www.preprints.org) | NOT PEER-REVIEWED | Posted: 7 August 2023 doi:10.20944/preprints202308.0512.v1

energy applied during ablation. In Figures S1a and S2a, Cl 2p and O 1s spectra of Samples A are presented, respectively. In both spectra, it is well seen that the peaks of Fe-Cl and Fe-O compounds are more intense than those of organic C-Cl and C-O species. This agrees well with the above discussed Fe spectrum of this sample (see Figure 8a) where Fe-Cl and Fe-O species were also detected. On the other hand, since the sample was prepared in chloroform, after which its NPs were drop-cast and kept in the air, the presence of organic C-Cl and C-O species on its surface was also expected.

Similarly, Cl 2p and O 1s spectra of Sample B prepared by ablation at 120 mJ/pulse are presented in Figures S1b and S2b. Here again one can observe intense peaks of Fe-O and Fe-Cl species as dominating components, which agrees well with the above-presented XPS Fe 2p spectrum (Figure 8b). The amount of organic C-Cl species is smaller in this sample, which is probably related to a smaller amount of chloroform absorbed on its surface.

Based on the above discussed XPS spectra, the NPs of both LAL-prepared samples are composed of a mixture of iron oxide and chloride phased, with a small fraction of metallic Fe phase inclusions. Quantitative analysis made by means of XPS demonstrated that the overall composition of both samples is very similar, as they have very close contents of iron, chlorine, and oxygen (see *Supplementary Materials* Figure S4). Thus, based on their composition (metallic iron, iron oxide and iron chloride species as main components), NPs of both samples are expected to be somewhat soluble and release Fe ions in contact with water. Thus, such NPs were concluded to be suitable for embedding into PLLA NSs.

3.3. XRD analysis of prepared NPs

XRD analysis was performed on the as-prepared Fe-containing NPs to examine their phase composition, with diffraction patterns of the samples being presented in Figure 9. Because numerous iron oxide/chloride phases exhibit quite close peak positions, and nanomaterials often contain high fractions of amorphous phase, determining the precise phase composition of the samples seems impossible. Nevertheless, in Figure 9 we show a set of most probable phases observed in the patterns of Samples A and B, which is generally consistent with the conclusions previously drawn from XPS measurements. More specifically, both samples were based on a mixture of iron-oxide and iron-chloride phases, in which both Fe(II) and Fe(III) species coexist. Interestingly, and in agreement with previous work reported by others [33,34,37–39,50], according to the XRD patterns, the main phase with the best-detected signals could be hematite (Fe_2O_3). As was found by XPS observations, the fraction of metallic Fe inclusions was quite small, which is why one cannot see metallic Fe in the XRD patterns.

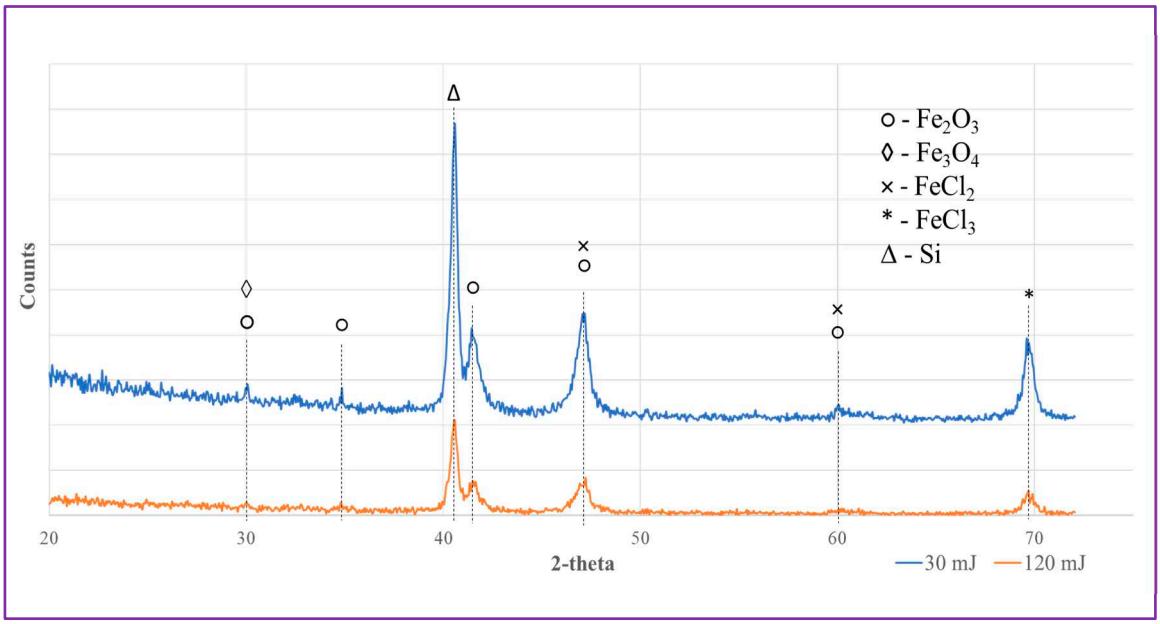

 doi:10.20944/preprints202308.0512.v1

Figure 9. XRD patterns of Samples A (blue) and B (orange) prepared at 30 (blue) and 120 mJ/pulse (orange) and deposited on Si wafer.

Thus, based on the above mentioned analyses, the NPs prepared by LAL method, both Samples A and B, were based on a mixture of iron chloride and oxide phases, with some metallic Fe(0) species as admixture. This was expected to make such NPs release Fe ions in water when PLLA nanosheets embedded with them were immersed into physiological solution at pH 7.4.

3.4. Ion release from NP-loaded NSs

Optical microscopy observations of prepared PLLA NSs incorporated with NPs (both cross-sectional and surface view) demonstrated that the NPs were fairly uniformly distributed in the prepared NSs, being entrapped during spin-coating as agglomerates into pockets of different sizes formed by spin-coated PLLA NSs (see *Supplementary Materials* Figures S4 and S5).

As seen in Figure S4, the thickness of PLLA NSs prepared in this study was mainly between ~80 and ~100 nm, indicating that all the NPs used by us were smaller and could be incorporated into such NSs. It was found that most of loaded NPs were entrapped as agglomerates into relatively large PLLA pockets, implying that the spin-coating process used to prepare such NSs is still to be optimized in the future in order to understand better how rotational speed, as well as concentrations of incorporated NPs and PLLA as polymer itself, influence the thickness and morphology of prepared NSs. Meanwhile, in this study, we mainly focused on the ability of the prepared PLLA NSs to release Fe ions in contact with physiological solution.

The ion release potential of nanosheets incorporated with Fe-containing NPs was tested by means of ICP-MS, for which the NSs were immersed in a buffer solution with pH 7.4 and kept at a temperature of 37°C, as shown in Figure 4. After certain periods of time, aliquots were taken in order to measure the concentration of released Fe (or/and) Zn ions. Figure 10 presents the results of ICP-MS measurements obtained for two PLLA NSs incorporated with Fe-containing NPs from Samples A (a) and B (b). In both cases, the prepared NSs were adjusted to incorporate comparable amounts of Fe atoms, which was controlled during spin-coating (~0.3 mg/mL of Fe in $CHCl_3$).

It is seen in Figure 10 that the concentration of Fe ions released by both NSs into physiological solution (pH 7.4) gradually increased during the first ~5 h of immersion into the liquid, after which the amount of released ions was quite constant for the next ~20 h of the experiment. The maximum level achieved was detected to be quite low, being on the order of just ~110 ppb/cm^2. However, here it should be noted that to date the optimum concentration of Fe ions on skin surface necessary to enhance burn wound healing is not known yet and still has to be determined. At the same time, the fact itself that the prepared PLLA nanosheets released Fe ions from their incorporated NPs as fast as after 5 h looks very promising, implying that in real life such dressings can provide some Fe ions on wound surface already after a few hours after their application. This looks very attractive, because typically dressings are used on wounds for as long as ~24 h before replacement, and therefore it is important for them to release their drugs or microelements within a reasonably short period of time.

Preprints (www.preprints.org) | NOT PEER-REVIEWED | Posted: 7 August 2023 doi:10.20944/preprints202308.0512.v1

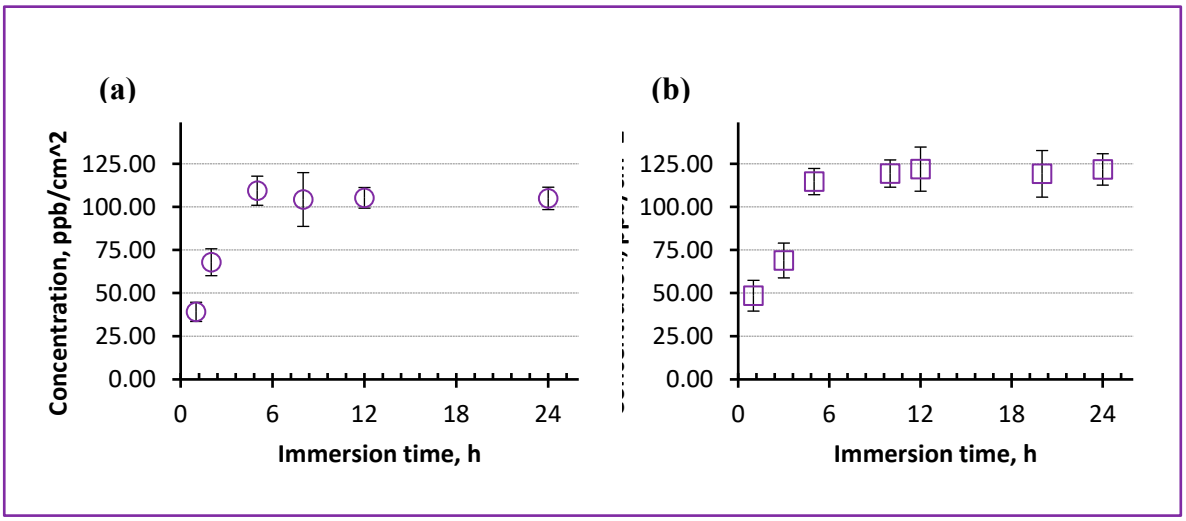

Figure 10. Concentration of Fe ions released by NSs incorporated with Fe-containing NPs laser-prepared at 30 (a) and 120 mJ/pulse (b). Both NSs were prepared using corresponding colloids with the same NP concentration (~ 0.3 mg/mL).

For comparison, at next stage, we also prepared NSs incorporated with both Fe and Zn ions, for which Sample B and commercial ZnO NPs were used. Figure 11 demonstrates how a PLLA NS embedded with two types of NPs released Fe (triangles) and Zn (diamonds) ions when immersed in physiological solution at pH 7.4. It is seen that different levels of concentration was achieved by Fe and Zn ions released by this NS which was intentionally embedded with different amounts of nanoparticles. Importantly, however, maximum level of both Fe and Zn ions was achieved after around 4-5 h of immersion. This probably implies that it is the permeability of the PLLA NS that played an important role in releasing ions of the two types. As mentioned above, the difference in released concentration of Fe and Zn ions can be explained by a different amount of NPs used during spin-coating. Here, we used the same concentration of Sample B to prepare this NS (0.3 mg/mL of Fe in chloroform), while 1.0 mg/mL of ZnO NPs was added into the same dispersion.

At the same time, for comparison, we also used commercially available iron oxide NPs (Fe_2O_3), which were incorporated into PLLA NSs at different concentrations and then analyzed by ICP-MS after their immersion in the solution. However, no noticeable level of Fe release was observed in their case, which would be detected by ICP-MS, agreeing well with insolubility of Fe_2O_3 in water.

Preprints (www.preprints.org) | NOT PEER-REVIEWED | Posted: 7 August 2023 doi:10.20944/preprints202308.0512.v1

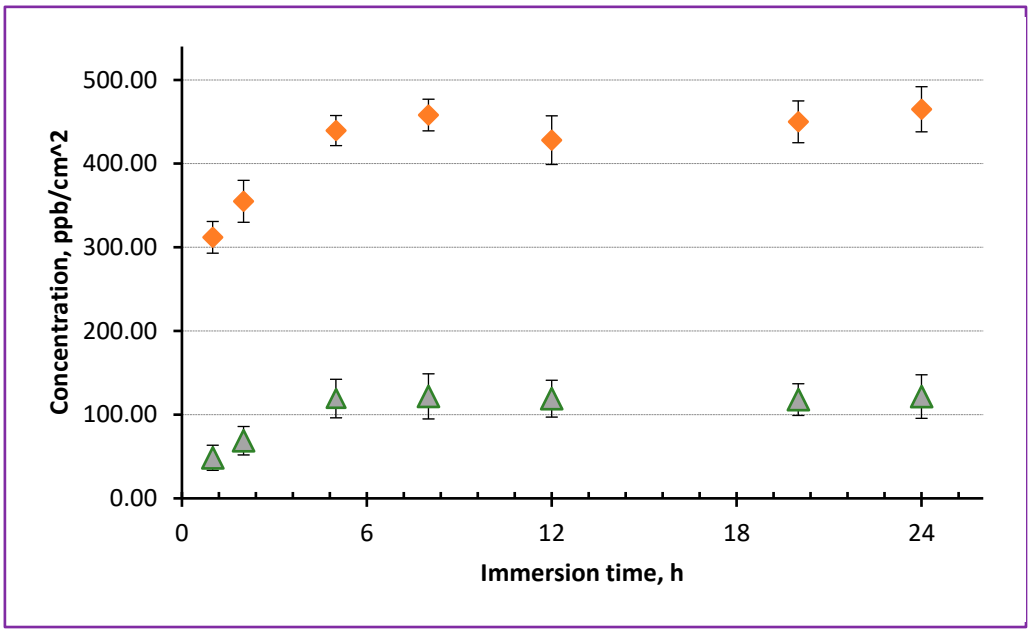

Figure 11. Concentration of Fe (triangles) and Zn (diamonds) ions released by NSs incorporated with two types of NPs. Sample B and commercial ZnO NPs (with sizes below 25 nm) were used as source of Fe and Zn ions, respectively.

The main focus of this study was on preparing Fe-containing NPs that would be soluble in water and release Fe ions. This task was quite challenging as iron oxides are known to have very low solubility in water. In addition, it should be added that thus far, the level on concentrations of microelements (such as Fe and Zn) desired in the wound area for efficient healing is not known yet and needs additional studies. That is why, here we only aimed to show that (1) water-soluble Fe-containing NPs capable of releasing ions could be prepared by laser ablation and then incorporated into biodegradable NSs; (2) two types of NPs with different metal ions (Fe and Zn) could be embedded simultaneously and then release their ions over time independently. At the same time, *in-vivo* tests on animals are needed to see how PLLA NSs incorporated with useful microelements can influence wound healing. Yet, the fact that several types of metal-ion containing NPs can be embedded into PLLA nanosheets, and that such ions are then independently released as fast as within several hours (up to 4-5) shows promise. It is obvious that wound dressings, when placed at wound area, should demonstrate their efficacy and contribute to healing-related processes within several hours.

4. Conclusions

Burn wound healing is known to be accelerated by presence of ions of certain microelements (including Fe and Zn). Aiming at developing inexpensive and easy-to-use patches for burn wounds, in this work, we prepared biodegradable polymer nanosheets of poly(L-lactic acid), PLLA loaded with Fe-containing nanoparticles which were generated by means of laser ablation in chloroform as medium. Such thin PLLA nanosheets incorporated with Fe-containing nanoparticles can release Fe ions in contact with skin, which should facilitate skin healing.

We first prepared water-soluble nanoparticles based on Fe ions via ablating iron plate by laser in chloroform. The method was chosen as we aimed at generating chloride/oxide based nanomaterials which would demonstrate solubility in contact with water. The prepared nanoparticles were found to be of proper sizes (below 100 nm) and based on Fe chloride and oxide phases, which made them suitable for incorporation into PLLA nanosheets via spin-coating. After characterization, the prepared Fe-containing nanomaterials were embedded into PLLA nanosheets which were fabricated via spin-coating. To test their ion-releasing properties, the prepared nanosheets

were immersed in a buffered liquid (pH 7.4) at +37 °C, where their Fe ion release was monitored over time.

In parallel, we also prepared PLLA nanosheets incorporated with two types of ions, Fe and Zn, to demonstrate that PLLA nanosheets can be loaded with reservoirs of several metal ions that are known to stimulate wound healing. Importantly, independent ion release was demonstrated by such nanosheets, with attractive ion release rates, which makes the prepared nanosheets promising for further development of biomedical materials on their bases.

Supplementary Materials: The following supporting information can be downloaded at the website of this paper posted on Preprints.org. Figure S1. XPS Cl 2p spectra of Fe-containing NPs in Samples A (a) and B (b). Figure S2. XPS O 1s spectra of Fe-containing NPs in Samples A (a) and B (b). Figure S3. Elemental composition of Samples A and B prepared by LAL (as calculated based on XPS results). Figure S4. Cross-secrional SEM images of PLLA NSs incorporated with NSs. The nanosheets were spin-coated on Si substrate and have ~190-nm-thick PVA under-layer. Figure S5. Surface images (SEM micrographs) of PLLA NSs loaded with Fe-containing and with ZnO NPs. Scale bar indicates 1 μm.

Author Contributions: Methodology, A.M., S.I., and S.A.K.; Conceptualization, S.A.K.; Investigation, A.M., M.E.T., N.M., A.A.A., D.A., and S.O.G.; Formal analysis, A.M., A.A.A., S.O.G., and A.B.; Supervision, N.M., S.I., and S.A.K.; Project administration, S.A.K. and S.I.; Data curation, A.A.A., D.A., S.I., and S.A.K.; Writing- original draft, A.M., N.M., A.B., and S.A.K.; Writing- review and editing, N.M., S.I. and S.A.K.

Funding: The research was financially supported by the Russian Foundation of Basic Research (RFBR) (grant no. RFBR 20-52-04005).

Acknowledgements: The research was financially supported by the Japan Society for the Promotion of Science (JSPS) (grant no. 16K04904). S.A.K. also thanks the support from the Amada Foundation (grant no. AF-2019225-B3).

Conflict of Interest: The authors declare no conflict of interest.

References

1. Lazurus, G.S.; Cooper, D.M.; Knighton, D.R.; Margolis, D.J.; Pecararo, R.E.; Rodeheaver, G., Robson, M.C. Definitions and guidelines for assessment of wounds and evaluation of healing. Arch. Dermatol. 1994, 130, 489-493. Doi: 10.1001/archderm.1994.01690040093015
2. Lin, P.H.; Sermersheim, M.; Li, H.C.; Lee, P.H.U.; Steinberg, S.; Ma, J. Zinc in wound healing modulation. Nutrients 2018, 10, 116. Doi: 10.3390/nu10010016
3. Cappuccio de Castro, K.; Silva, E.K.; Nogueira Campos, M.G.; Innocentini Mei, L.H. Hyaluronic acid/polyvinyl alcohol electrospun nanofiber membranes loaded with plantago major extract for smart wound dressings. ACS Appl. Nano Mater. 2022, 5, 12616−12625. Doi: 10.1021/acsanm.2c02402
4. Bandeira, M.; Chee, B.S.; Frassini, R.; Nugent, M.; Giovanela, M.; Roesch-Ely, M.; Crespo, J.S.; Devine, D.M. Antimicrobial PAA/PAH electrospun fiber containing green synthesized zinc oxide nanoparticles for wound healing. Materials 2021, 14, 2889. Doi: 10.3390/ma14112889
5. Abdollahi, Z.; Zare, E.N.; Salimi, F.; Goudarzi, I.; Tay, F.R.; Makvandi, P. Bioactive carboxymethyl starch-based hydrogels decorated with CuO nanoparticles: Antioxidant and antimicrobial properties and accelerated wound healing in vivo. Int. J. Mol. Sci. 2021, 22, 2531. Doi: 10.3390/ijms22052531
6. Basit, H.M.; Ali, M.; Shah, M.M.; Shah, S.U.; Wahab, A.; Albarqi, H.A.; Alqahtani, A.A.; Walbi, I.A.; Khan, N.R. Microwave enabled physically cross linked sodium alginate and pectin film and their application in combination with modified chitosan-curcumin nanoparticles. A novel strategy for 2nd degree burns wound healing in animals. Polymers 2021, 13, 2716. Doi: 10.3390/polym13162716
7. Reczyńska-Kolman, K.; Hartman, K.; Kwiecień, K.; Brzychczy-Włoch, M.; Pamuła, E. Composites based on gellan gum, alginate and nisin-enriched lipid nanoparticles for the treatment of infected wounds. Int. J. Mol. Sci. 2022, 23, 321. Doi: 10.3390/ijms23010321
8. Nawaz, T.; Iqbal, M.; Khan, B.A.; Nawaz, A.; Hussain, T.; Hosny, K.M.; Abualsunun, W.A.; Rizg, W.Y. Development and optimization of acriflavine-loaded polycaprolactone nanoparticles using box–behnken design for burn wound healing applications. Polymers 2022, 14, 101. doi: 10.3390/polym14010101
9. Verbelen, J.; Hoeksema, H.; Heyneman, A.; Pirayesh, A.; Monstrey, S. Aquacel® Ag dressing versus Acticoat™ dressing in partial thickness burns: A prospective, randomized, controlled study in 100 patients. Part 1: Burn wound healing. Burns 2014, 40, 416-427. Doi: 10.1016/j.burns.2013.07.008
10. He, C.H.; Yu, B.R.; Lv, Y.C.; Huang, Y.F.; Guo, J.D.; Li, L.; Chen, M.M.; Zheng, Y.Q.; Liu, M.H.; Guo, S.B.; Shi, X.N.; Yang, J.M. Biomimetic asymmetric composite dressing by electrospinning with aligned

nanofibrous and micropatterned structures for severe burn wound healing. ACS Appl. Mater. Interfaces 2022, 14, 32799-32812. Doi: 10.1021/acsami.2c04323
11. Ishak, M.Q.H.; Shankar, P.; Turabayev, M.E.; Kondo, T.; Honda, M.; Gurbatov, S.O.; Okamura, Y.; Iwamori, S.; Kulinich, S.A. Biodegradable polymer nanosheets incorporated with Zn-containing nanoparticles for biomedical applications. Materials 2022, 15, 8101. Doi: 10.3390/ma15228101
12. Li, J.; Wang, C.; Han, X.S.; Liu, S.; Gao, X.; Guo, C.L.; Wu, X.C. Aramid nanofibers-reinforced rhein fibrous hydrogels as antibacterial and anti-inflammatory burn wound dressings. ACS Appl. Mater. Interfaces 2022, 14, 45167−45177. Doi: 10.1021/acsami.2c12869
13. Kaul, S.; Sagar, P.; Gupta, R.; Garg, P.; Priyadarshi, N.; Singhal, N.K. Mechanobactericidal, gold nanostar hydrogel-based bandage for bacteria-infected skin wound healing. ACS Appl. Mater. Interfaces 2022, 14, 44084−44097. Doi: 10.1021/acsami.2c10844
14. Patten, J.A. Nutrition and would healing. J. Greater Houston Dent. Soc. 1998, 69, 14-15.
15. Guo, S.; DiPietro, L.A. Factors affecting wound healing. J. Dent. Res. 2010, 89, 219-229. Doi: 10.1177/0022034509359125
16. Kavalukas, S.L.; Barbul, A. Nutrition and would healing: An update. Plast. Reconstr. Surg. 2011, 127, 38S-43S. Doi: 10.1097/PRS.0b013e318201256c
17. Fujie, T.; Ricotti, L.; Desii, A.; Menciassi, A.; Dario, P.; Mattoli, V. Evaluation of substrata effect on cell adhesion properties using freestanding poly(l-lactic acid) nanosheets. Langmuir 2011, 27, 13173-13182. Doi: 10.1021/la203140a
18. Okamura, Y.; Nagase, Y. Fabrication of bio-friendly polymer nanosheets for biomedical applications. Trans. Mat. Res. Soc. Japan 2014, 39, 379-384.
19. Okamura, Y.; Nagase, Y.; Takeoka, S. Patchwork coating of fragmented ultra-thin films and their biomedical applications in burn therapy and antithrombotic coating. Materials 2015, 8, 7604-7614. Doi: 10.3390/ma8115404
20. Okamura, Y.; Kabata, K.; Kinoshita, M.; Miyazaki, H.; Saito, A.; Fujie, T.; Ohtsubo, S.; Saitoh, D.; Takeoka, S. Fragmentation of poly(lactic acid) nanosheets and patchwork treatment for burn wounds. Adv. Mater. 2013, 25, 545-551. Doi: 10.1002/adma.201202851
21. Kim, M.J.; Osone, S.; Kim, T.S.; Higashi, H.; Seto, T. Synthesis of nanoparticles by laser ablation: A review. KONA Powder Part. J. 2017, 34, 80-90. Doi: 10.14356/kona.2017009
22. Svetlichnyi, V.A.; Shabalina, A.V.; Lapin, I.N.; Goncharova, D.A.; Velikanov, D.A.; Sokolov, A.E. Characterization and magnetic properties study for magnetite nanoparticles obtained by pulsed laser ablation in water. Appl. Phys. A 2017, 123, 763. Doi: 10.1007/s00339-017-1390-7
23. Timofeev, K.L.; Kharlamova, T.S.; Ezhov, D.M.; Salaev, M.A.; Svetlichnyi, V.A.; Vodyankina, O.V. Hydroxymethylfurfural oxidation over unsupported Pd-Au alloy catalysts prepared by pulsed laser ablation: Synergistic and compositional effects. Appl. Catal. A 2023, 656, 119121. Doi: 10.1016/j.apcata.2023.119121
24. Shabalina, A.V.; Svetlichnyi, V.A.; Kulinich, S.A. Green laser ablation-based synthesis of functional nanomaterials for generation, storage and detection of hydrogen. Curr. Opin. Green Sustainable Chem. 2022, 33, 100566. Doi: 10.1016/j.cogsc.2021.100566
25. Mintcheva, N.; Subbiah, D.K.; Turabayev, M.E.; Gurbatov, S.O.; Rayappan, J.B.B.; Kuchmizhak, A.A.; Kulinich, S.A. Gas sensing of laser-produced hybrid TiO2-ZnO nanomaterials under room-temperature conditions. Nanomaterials 2023, 13, 670. Doi: 10.3390/nano13040670
26. Shabalina, A.V.; Fakhrutdinova, E.D.; Golubovskaya, A.G.; Kuzmin, S.M.; Koscheev, S.V.; Kulinich, S.A.; Svetlichnyi, V.A.; Vodyankina, O.V. Laser-assisted preparation of highly-efficient photocatalytic nanomaterial based on bismuth silicate. Appl. Surf. Sci. 2022, 575, 151732. Doi: 10.1016/j.apsusc.2021.151732
27. Shankar, P.; Ishak, M.Q.H.; Padarti, J.K.; Mintcheva, N.; Iwamori, S.; Gurbatov, S.O.; Lee, J.H.; Kulinich, S.A. ZnO@graphene oxide core@shell nanoparticles prepared via one-pot approach based on laser ablation in water. Appl. Surf. Sci. 2020, 531, 147365. Doi: 10.1016/j.apsusc.2020.147365
28. Fakhrutdinova, E.; Reutova, O.; Maliy, L.; Kharlamova, T.; Vodyankina, O.; Svetlichnyi, V. Laser-based synthesis of TiO2-Pt photocatalysts for hydrogen generation. Materials 2022, 15, 7413. Doi: 10.3390/ma15217413
29. Gurbatov, S.O.; Modin, E.; Puzikov, V.; Tonkaev, P.; Storozhenko, D.; Sergeev, A.; Mintcheva, N.; Yamaguchi, S.; Tarasenka, N.; Chivilin, A.; Makarov, S.; Kulinich, S.A.; Kuchmizhak, A.A. Black Au-decorated TiO2 produced via laser ablation in liquid. ACS Appl. Mater. Interfaces 2021, 13, 6522-6531. Doi: 10.1021/acsami.0c20463
30. Nemoykina, A.L.; Shabalina, A.V.; Svetlichnyi, A.V., Restoration and conservation of old low-quality book paper using aqueous colloids of magnesium oxyhydroxide obtained by pulsed laser ablation. J. Cult. Heritage 2019, 39, 42-48. Doi: 10.1016/j.culher.2019.03.003

31. Tarasenka, N.; Shustava, E.; Butsen, A.; Kuchmizhak, A.A.; Pashayan, S.; Kulinich, S.A.; Tarasenko, N. Laser-assisted fabrication and modification of copper and zinc oxide nanostructures in liquids for photovoltaic applications. Appl. Surf. Sci. 2021, 554, 149570. Doi: 10.1016/j.apsusc.2021.149570
32. Honda, M.; Kondo, T.; Owashi, T.; Shankar, P.; Ichikawa, Y.; Iwamori, S.; Kulinich, S.A. Nanostructures prepared via laser ablation of tin in water. New J. Chem. 2017, 41, 11308-11316. Doi: 10.1039/C7NJ01634D
33. Svetlichnyi, V.A.; Shabalina, A.V.; Lapin, I.N., Structure and properties of nanocrystalline iron oxide powder prepared by the method of pulsed laser ablation. Russ. Phys. J. 2017, 59, 2012–2016. Doi: 10.1007/s11182-017-1008-8
34. Shabalina, A.V.; Sharko, D.O.; Korsakova, D.R.; Svetlichnyi, V.A. Iron oxide nanopowders obtained via pulsed laser ablation, for supercapacitors. Russ. J. Inorg. Chem. 2020, 65, 271–278. Doi: 10.1134/S003602362002014X
35. Goncharova, D.A.; Bolbasov, E.N.; Nemoykina, A.L.; Aljulaih, A.A.; Tverdokhlebova, T.S.; Kulinich, S.A.; Svetlichnyi, V.A. Structure and properties of biodegradable PLLA/ZnO composite membrane produced via electrospinning. Materials 2021, 14, 2. Doi: 10.3390/ma14010002
36. Svetlichnyi, V.A.; Shabalina, A.V.; Lapin, I.N.; Goncharova, D.A.; Velikanov, D.A.; Sokolov, A.E. Study of iron oxide magnetic nanoparticles obtained via pulsed laser ablation of iron in air. Appl. Surf. Sci. 2018, 462, 226–236. Doi: 10.1016/j.apsusc.2018.08.116
37. Svetlichnyi, V.A.; Shabalina, A.V.; Lapin, I.N.; Goncharova, D.A.; Kharlamova, T.S.; Stadnichenko, A.I. Comparative study of magnetite nanoparticles obtained by pulsed laser ablation in water and air. Appl. Surf. Sci. 2019, 467-468, 402-410. Doi: 10.1016/j.apsusc.2018.10.189
38. Maneeratanasarn, P.; Khai, T.V.; Kim, S.Y.; Choi, B.G.; Shim, K.B. Synthesis of phase-controlled iron oxide nanoparticles by pulsed laser ablation in different liquid media. Phys. Status Solidi A, 2013, 210, 563-569. Doi: 10.1002/pssa.201228427
39. Fazio, E.; Santoro, M.; Lentini, G.; Franco, D.; Guglielmino, S.P.P.; Neri, F. Iron oxide nanoparticles prepared by laser ablation: synthesis, structural properties and antimicrobial activity. Colloids Surf. A, 2016, 490, 98-103. Doi: 10.1016/j.colsurfa.2015.11.034
40. De Bonis, A.; Lovaglio, T.; Galasso, A.; Santagata, A.; Teghil, R. Iron and iron oxide nanoparticles obtained by ultra-short laser ablation in liquid. Appl. Surf. Sci., 2015, 353, 433-438. Doi: 10.1016/j.apsusc.2015.06.145
41. Honda, M.; Goto, T.; Owashi, T.; Rozhin, A.G.; Yamaguchi, S.; Ito, T.; Kulinich, S.A. ZnO nanorods prepared via ablation of Zn with millisecond laser in liquid media. Phys. Chem. Chem. Phys. 2016, 18, 23628 -23637. Doi: 10.1039/C6CP04556A
42. Kondo, T.; Sato, Y.; Kinoshita, M.; Shankar, P.; Mintcheva, N.N.; Honda, M.; Iwamori, S.; Kulinich, S.A. Room temperature ethanol sensor based on ZnO prepared via laser ablation in water. Jpn. J. Appl. Phys. 2017, 56, 080304. Doi: 10.7567/JJAP.56.080304
43. Mintcheva, N.; Yamaguchi, S.; Kulinich, S.A. Hybrid TiO2-ZnO nanomaterials prepared by laser ablation in liquid method. Materials 2020, 13, 719. Doi: 10.3390/ma13030719
44. Fakhrutdinova, E.D.; Shabalina, A.V.; Gerasimova, M.A.; Nemoykina, A.L.; Vodyankina, O.V.; Svetlichnyi, V.A. Highly defective dark nano titanium dioxide: Preparation via pulsed laser ablation and application. Materials 2020, 13, 2054. Doi: 10.3390/ma13092054
45. Gurbatov, S.O.; Puzikov, V.; Storozhenko, D.; Modin, E.; Mitsai, E.; Cherepakhin, A.; Shevlyagin, A.; Gerasimenko, A.V.; Kulinich, S.A.; Kuchmizhak, A.A. Multigram-scale production of hybrid Au-Si nanomaterials by laser ablation in liquid (LAL) for temperature-feedback optical nanosensing, light-to-heat conversion, and anticounterfait labeling. ACS Appl. Mater. Interfaces 2023, 15, 3336-3347. Doi: 10.1021/acsami.2c18999
46. Sutthavas, P.; Schumacher, M.; Zheng, K.; Habibovic, P.; Boccaccini, A.R.; van Rijt, S. Zn-loaded and calcium phosphate-coated degradable silica nanoparticles can effectively promote osteogenesis in human mesenchymal stem cells. Nanomaterials 2022, 12, 2918. Doi: 10.3390/nano12172918
47. Lopes, J.H.; Souza, L.P.; Domingues, J.A.; Ferreira, F.V.; de Alencar Hausen, M.; Camilli, J.A.; Martin, R.A.; de Rezende Duek, E.A.; Mazli, I.O.; Bertran, C.A. In vitro and in vivo osteogenic potential of niobium-doped 45S5 bioactive glass: A comparative study. J. Biomed. Mater. Res. B 2020, 108B, 1372–1387. Doi: 10.1002/jbm.b.34486ss
48. Sukhorukova, I.V.; Sheveyko, Kiryukhantsev-Korneev, P.V.; Shtansky, D.V. Kinetics of Ag+ ion release from TiCaPCON-Ag films: Influence of Ag content and surface roughness. Adv. Biomater. Devices Med. 2015, 2, 37-43.
49. Khare, V.; Kraupper, A.; Mantion, A.; Jelicic, A.; Thunemann, A.F.; Giordano, C.; Taubert, A., Stable iron carbide nanoparticle dispersions in [Emim][SCN] and [Emim][N(CN)2] ionic liquids. Langmuir, 2010, 26, 10600-10605. Doi: 10.1021/la100775m
50. Amendola, V.; Riello, P.; Meneghetti, M. Magnetic nanoparticles of iron carbide, iron oxide, iron@iron oxide, and metal iron synthesized by laser ablation in organic solvents, J. Phys. Chem. C 2011, 115, 5140-5146. Doi: 10.1021/jp109371m

 doi:10.20944/preprints202308.0512.v1